Vertical extrapolation of Mars magnetic potentials

Donna M. Jurdy and Michael Stefanick
Department of Geological Sciences, Northwestern University, Evanston, Illinois, USA

Received 9 April 2004; revised 25 June 2004; accepted 22 July 2004; published 15 October 2004.

[1] Mars Global Surveyor (MGS) measured the most strongly magnetized crust in the heavily cratered southern hemisphere of Mars. Our analysis concentrates on the magnetic lineations or patterns centered near latitude 40°S, longitude 180°W, with a range of values ±40°, using a rotated Cartesian coordinate system. We downward continued the magnetic field measured at ~400 km elevation and very closely match the corresponding component measured during the aerobraking phase at altitudes extending down to ~100 km. Using the vertical component of the magnetic field alone, we construct a unique scalar potential and independently obtain from the derivatives of this scalar potential the x and y components of the field. These derived components agree very well with the observed horizontal components. This demonstrates the validity and utility of the method and the Cartesian approximation, and also it confirms the consistency of the MGS magnetic data set. A model constructed with just 8 vertical dipoles accounts for 80% of the variance of the scalar potential at 400 km over the region analyzed, but 14 dipoles can account for only 64% of the variance at 100 km. We also construct the vector potential, the curl of which generates the three components of the magnetic field. This more complicated description may contain more physical meaning than the scalar potential. The vector potential shows abrupt changes in direction over the analyzed region, suggesting either different stages of magnetization or local demagnetization. *INDEX TERMS:* 5440 Planetology: Solid Surface Planets: Magnetic fields and magnetism; 5420 Planetology: Solid Surface Planets: Impact phenomena (includes cratering); 6225 Planetology: Solar System Objects: Mars; *KEYWORDS:* magnetic, Mars, models

Citation: Jurdy, D. M., and M. Stefanick (2004), Vertical extrapolation of Mars magnetic potentials, *J. Geophys. Res.*, *109*, E10005, doi:10.1029/2004JE002277.

1. Introduction

[2] The Mars Global Surveyor Magnetic field and Electron Reflectometer Investigation (MAG/ER) measured unexpectedly strong magnetic fields due to an intensely magnetized crust during its low-altitude, aerobraking phase in 1997 [*Acuna et al.*, 1999]. Mars does not currently have a magnetic field, so the remanent magnetism must be a relic of a planetary field earlier in its history. The strongest magnetic lineations are located in the more heavily cratered southern highlands, centered at 180°W ± 30°. There, ten or more magnetic bands 100–200 km wide, possibly due to magnetic reversals, extend up to 2000 km in length [*Connerney et al.*, 1999]. Other weaker magnetic sources are scattered over much of the planet's surface. The intensity of Mars remanent magnetization reaches about 10 times that observed on and about Earth, on average. This requires both very strongly magnetic rocks and magnetization through a large section of the crust, possibly to a depth of 30 km for magnetization intensity ±20 A/m [*Connerney et al.*, 1999]. *Parker* [2003] models the distribution of magnetization to establish the lowest intensity possible and finds a value of 5 A/m for a 50 km layer. The magnetization intensity can not be well-constrained; only the product of the magnetization and thickness can be established. This product of the intensity and thickness for Mars' magnetization far exceeds the corresponding values anywhere on Earth, either for continental igneous provinces or newly formed ocean floor [*Parker*, 2003]. The disturbance near large impact craters requires that magnetization came before the impacts [*Acuna et al.*, 1999; *Nimmo and Gilmore*, 2001] in the Noachian epoch of Mars' history ~4 Ga. Demagnetization has been shown to extend beyond the immediate crater, even out to several radii [*Mitchell et al.*, 2003]. A mechanism for pressure-induced demagnetization of pyrrhotite in the Martian crust could account for the pattern of demagnetization near large craters [*Rochette et al.*, 2003].

[3] In our study, we focus on magnetic lineations in the southern hemisphere centered near latitude 40°S, longitude 180°W. We analyze observations acquired in this region to determine the pattern and characteristics of magnetization. Using two-dimensional Fourier analysis, we downward continue the field from satellite mapping altitude at ~400 km to 100 km altitude for comparison with measurements acquired during the initial aerobraking phase of MGS. With this, we model the observed field, matching the scalar magnetic potential with a set of vertical dipoles, and compare with surface stratigraphy and geological features such as ancient craters and faults.

0148-0227/04/2004JE002277$09.00

In addition, we construct a vector potential field which may contain greater physical meaning than the scalar potential. Further characterization of the strong southern hemisphere magnetization could clarify the nature and timing of Mars' magnetic field.

2. Analysis

[4] We began our study of Mars' magnetic lineations with an analysis of the MAG/ER data. *Connerney et al.* [2001] have made available data from the mapping phase of MGS which measured the vector components of the magnetic field at altitudes of 404 km ±30 km, covering almost the entire planet. In our analysis we used data given on the Web site http://mgs-mager.gsfc.nasa.gov/publications/grl_28_connerney/data/. Here, these data have been conveniently averaged, decimated, sorted and binned into 180 latitude and 360 longitude bins by degree, providing estimates of each component in a spherical coordinate system with r (radial), ϕ (east-west) and θ (north-south) components.

[5] We consider the subset of data within ±40° of 40°S and 180°, i.e., longitudes 140° to 220°, latitudes 0° to −80°. We then convert these latitudes and longitudes to Cartesian coordinates and use an ordinary two-dimensional Fourier analysis for downward continuation (we omit technical details). We emphasize that we use this approximation with the Cartesian variables, x, y, z rather than the usual spherical variables, ϕ, θ, r. This approximation neglects the curvature of the surface and may seem coarse, but we will show that the components of the original magnetic field agree very nicely with those computed from the gradient of the derived scalar potential.

[6] This region, 40°S ± 40°, 180°W ± 40°, covers nearly an octant of the planet and encompasses the most strongly magnetized crust on Mars. Our goal is to describe the magnetic field by means of scalar and vector potentials because they are simpler, smoother and more fundamental than working with the three components of the magnetic field. The magnetic field components can be described by the gradient of a scalar potential or by the curl of a vector potential. Each version can be modeled.

2.1. Vertical Extrapolation

[7] Fourier analysis methods, as described by *Kanasewich* [1975, pp. 92–94] can be used to extrapolate from satellite mapping altitudes (400 km) to aerobraking altitudes (100 km). Figures 1a, 1b, and 1c show the magnetic field components B_z, B_y, and B_x extrapolated, or downward continued, to 100 km. In Figure 2a we show the magnetic field components B_z at 400 km, the average MGS mapping altitude level. For comparison, the downward continued field, B_z (Figure 1a), is shown in Figure 2b superposed upon the radial component of the field, B_r, measured at ∼100 km during the aerobraking phase of MGS [*Acuna et al.*, 1999]. Downward continuation, essentially a differencing operation, is very sensitive to errors in measurement and therefore often approached with caution. However, the downward continued field is in excellent agreement with actual observations acquired at low altitude (Figure 2b), and fills in all data gaps. The Martian geology was scanned and reprojected from the USGS geological maps of Mars

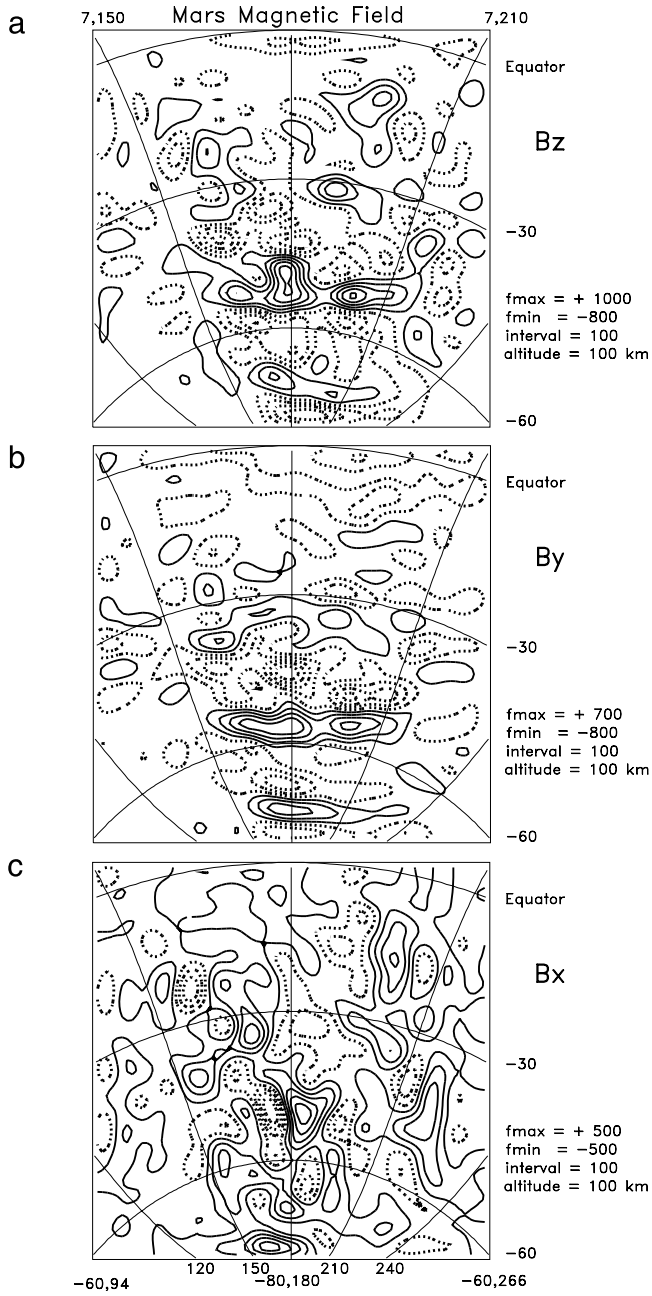

Figure 1. (a) The vertical component of the magnetic field B_z extrapolated downward from 400 to 100 km using a Fourier transform. Solid lines contour positive values; dashed lines used for negative values. Map centered at 40°S, 180°W, extending 40° in each direction. Latitude and longitude lines shown for reference with the geographical coordinates of the corners given. (b) The north-south component of the magnetic field, B_y, extrapolated downward to 100 km, as in Figure 1a. (c) The east-west component of the magnetic field, B_x, extrapolated downward to 100 km, as in Figure 1a.

[*Greeley and Guest*, 1997; *Scott and Tanaka*, 1997; *Tanaka and Scott*, 1997] of the same area and is shown for reference in Figure 2c using the same map projection as used for other figures. Highland terrain materials with some younger northern channel materials and southern polar deposits

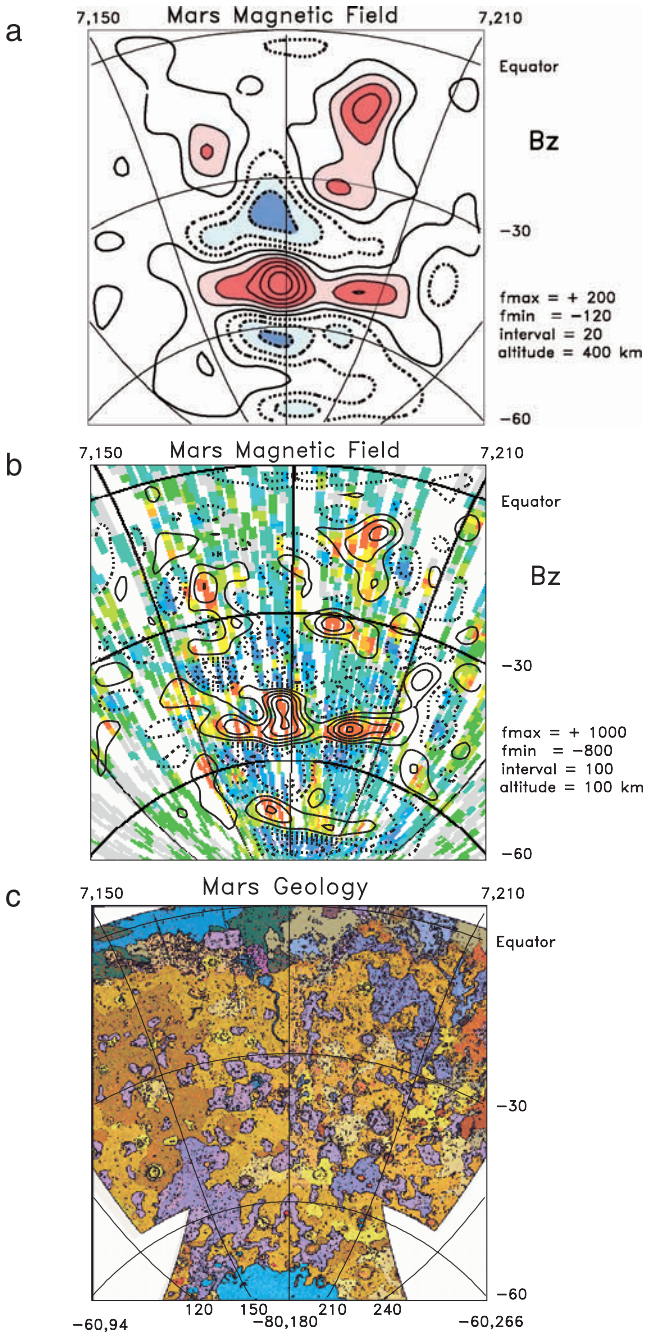

Figure 2. (a) The vertical component of the magnetic field B_z as measured at 400 km. Map projection as in Figure 1. (b) The vertical component of the magnetic field B_z extrapolated downward from 400 to 100 km using a Fourier transform. The result agrees very well with aerobraking data obtained at 100 km (shown in color) and fills in data gaps. Aerobraking data: red, strongly positive; blue, strongly negative. (c) Geology of Mars' highland terrain. Colors: brown/tan, Noachian Plateau Sequence; purple, Ridged Unit; blue, Channel Material north and Polar Deposits south; red, Volcanic Assemblage [*Greeley and Guest*, 1997; *Scott and Tanaka*, 1997; *Tanaka and Scott*, 1997]. Map projection as in Figure 1.

cover the region analyzed. These include the predominant units: Plateau Sequence (Npld, Npl_1, Npl_2, Hpl_3), Western Volcanic Assemblage (Aht_3, Ht_1, Ht_2), Ridged Unit and Ridged Plains Material (Nplr, Hr), and recent surficial layers: Channel System Materials (Achu) and Polar Deposits (Apl).

2.2. Scalar Potential

[8] The scalar potential can be directly constructed from the vertical component of the magnetic field in a Cartesian representation. We take the Fourier transform of B_z, and divide by the vertical wave number, k_z, which is the square root of the sum of the squares of the horizontal wave numbers [*Blakely*, 1996, pp. 65–97]. This gives the scalar potential, V. Fourier transforms are shown with circumflections.

$$\vec{B} = \nabla V$$
$$\hat{V} = \frac{\hat{B}_z}{k_z} = \frac{\hat{B}_z}{\sqrt{k_x^2 + k_y^2}} \qquad (1)$$
$$B_x = \frac{\partial V}{\partial x} \;\; ; \;\; B_y = \frac{\partial V}{\partial y}.$$

[9] At first sight, the scalar potential, V, seems superior because a single component describes horizontal components of the magnetic field as gradients, and the potential itself is a smoothed version of the vertical component. The constructed scalar potential field at 100 km is shown in Figure 3a. The resulting horizontal magnetic components, B_y and B_x, shown in Figures 3b and 3c can then be compared with the original horizontal components rotated into this coordinate system (Figures 1b and 1c). The corresponding fields are nearly identical, as seen by comparing the original horizontal components of the magnetic field (Figures 1b and 1c) with the constructed components (Figures 3b and 3c). This agreement constitutes an independent check of the method as the horizontal components of the magnetic field were not used to construct the scalar potential. The small differences in the corresponding fields are due, we believe, to the Cartesian approximation used and the use of a finite difference for the derivatives. Importantly, this confirms the internal consistency of the components of the magnetic field, as well as the overall analysis. An error in any one of the magnetic field components would not allow construction of a scalar potential with these properties.

[10] The scalar potential field, V, shows a simple pattern in the area 40°S, 180°W ± 40° (Figure 3a), with a pattern that appears to be more equidimensional than linear in form. Using two-dimensional Fourier analysis, the scalar potential field is downward-continued from satellite level to a lower one for comparison with surface features. Figure 4a shows the surface scalar potential field along with the three ancient impact basins in this region identified by *Schultz et al.* [1982]. The multiring basins from north to south identified are Al Qahira, S. of Hesphaestus Fossae, and Sirenum. These eroded features no longer retain the ejecta or topographic signature of fresh craters, but may be identified by concentric basins and outflow channels. (These circular features can be compared with the Martian surface geology in Figure 2c.) Similarly, in the northern lowlands, *Frey et al.* [2002] have identified numerous circular features retaining little evidence of structure that they infer to be ancient

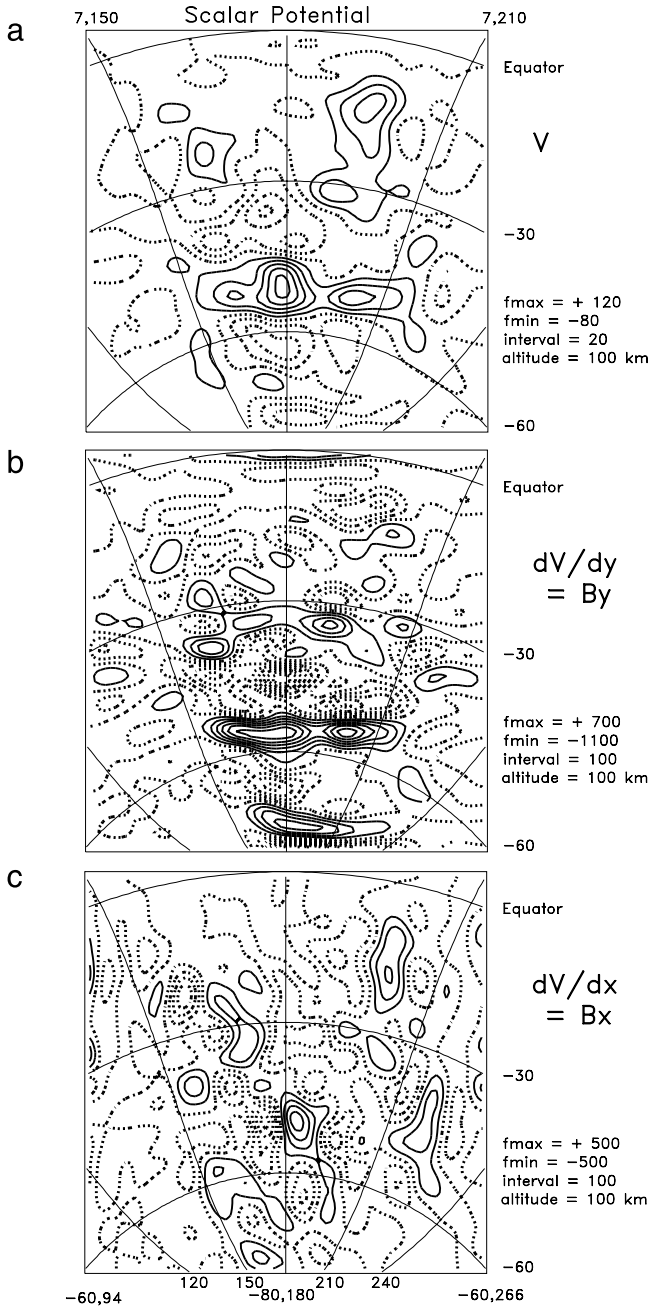

Figure 3. (a) The magnetic scalar potential obtained from the vertical component of the magnetic field using a Fourier transform and extrapolated downward from 400 to 100 km. The gradient components of this field shown in Figures 3b and 3c replicate the horizontal components of the magnetic field almost perfectly. Map projection as in Figure 1. (b) The y derivative of the scalar potential, V, at 100 km for comparison with B_y in Figure 1b. (c) The x derivative of the scalar potential, V, at 100 km for comparison with B_x in Figure 1c.

buried impact craters. Here in the southern hemisphere region analyzed, the strongest values of the scalar potential lie adjacent to the rings of the ancient craters, though not actually within the rings. In particular, for the southernmost structure with the Sirenum basin, the scalar potential contour lines appear to curve around the outermost 1000 km ring as identified by *Schultz et al.* [1982]. This curvature of scalar potential contour lines around the Sirenum Basin circles becomes most apparent when the field is downward continued to near surface level (Figure 4a).

2.3. Models for Scalar Potential

[11] The discrete appearance of the scalar potential field (Figure 3a) suggests it can be successfully modeled with isolated dipoles. We construct a multiple dipole model that approximates the scalar potential. To do this we position vertical dipoles at the peaks and troughs of the scalar potential field, iteratively adjusting locations to maximize the fit as measured by the variance. Additional dipoles are added until the improvement in fit levels. The scalar potential is summed for n vertical dipoles:

$$V(x,y,z) = \sum_{m=1}^{n} q_m (z - z_m) s_m^{-3}$$
$$s_m = \sqrt{(x - x_m)^2 + (y - y_m)^2 + (z - z_m)^2}, \quad (2)$$

where q_m is the source strength and s_m is the distance between the field point and the mth source point.

[12] With vertical dipoles we determine depths and magnitudes for selected centers and average surroundings, and at the satellite mapping level of 400 km (Figure 2a) we find that 8 sources can account for 80% of the variance (correlation coefficient ~0.89). (At this level only 4 sources already account for >60% of the variance.) These sources range in depth 260 ± 30 km, but the source magnitudes range over a factor of 4. Using the autocorrelation of the scalar potential, we estimate that there are only 20–30 independent components of the field (which corresponds to a resolution of 4 × 5 or 5 × 6). As we extrapolate downward, the continued field is much noisier than the field at satellite level. More centers become evident, and thus for modeling more centers are necessary to account for a given partial variance. For example, at aerobraking altitudes (100 km), 14 centers account for 64% of the variance (correlation coefficient = 0.80). The scalar potential for the best fitting dipoles is shown in Figure 4b for the case of 14 dipoles to be compared with the scalar potential in Figure 3a. No obvious relation of the dipole locations and surface geology (Figure 2c) is apparent. At Mars' surface still more dipoles, greater than 20, are required to fit the scalar potential field (Figure 4a), and the fit is poorer. At any altitude, as more centers are included they begin to overlap, and the improvement in fit slows and then worsens. This description will be a topic for further research.

[13] The depths of the best fitting dipoles (down to 200+ km beneath the surface) are not geologically realistic. Certainly temperatures at this depth would prohibit magnetization. In their analysis of an isolated at magnetized region located 35°S, 295°E, *Connerney et al.* [2001] find a possible source of a nearly vertical dipole with a depth of 106 km, but they note that other models would fit equally well. *Langlais et al.* [2004] model Mars' magnetic field with equivalent source dipoles, assuming a 40 km thick magnetized layer. The depth, intensity, and direction of magnetization can only be uniquely determined with in situ measurements and additional constraints.

2.4. Vector Potential

[14] The vector potential, though more challenging to illustrate, is more intuitive in the sense that it represents the field as a swirl around an axis rather than a flow from a (nonexistent) monopole to another opposite monopole as the scalar potential does. The vector potential, $\vec{A}$, is not unique since we can always add a gradient of a scalar field and obtain a new vector potential which generates the same magnetic field components (since the curl of a gradient is always zero).

$$\begin{aligned} \vec{B} &= \nabla \times \vec{A} \\ \hat{A}_x &= \frac{\hat{B}_y}{k_z} = \frac{\hat{B}_y}{\sqrt{k_x^2 + k_y^2}} \\ \hat{A}_y &= -\frac{\hat{B}_x}{k_z} = -\frac{\hat{B}_x}{\sqrt{k_x^2 + k_y^2}} \\ \hat{A}_z &= 0. \end{aligned} \tag{3}$$

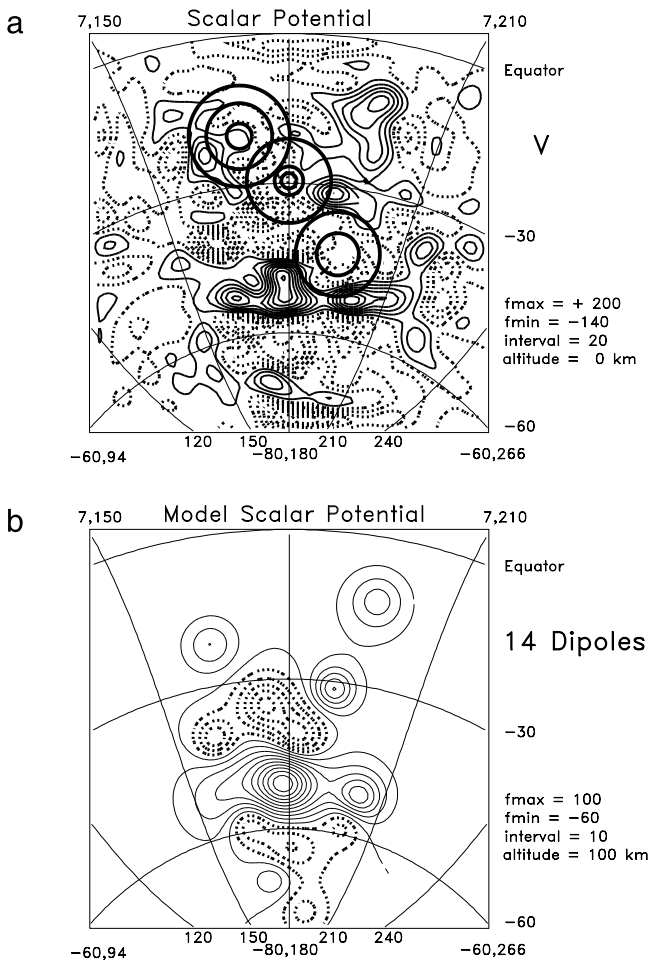

Figure 4. (a) The magnetic scalar potential extrapolated downward to the surface of Mars. Also shown as concentric circles are ancient impact basins [*Schultz et al.*, 1982]. Multiring basins from north to south: Al Qahira, south of Hesphaestus Fossae, Sirenum. Map projection as in Figure 1. (b) The magnetic scalar potential for 14 best fitting vertical dipoles extrapolated downward to 100 km.

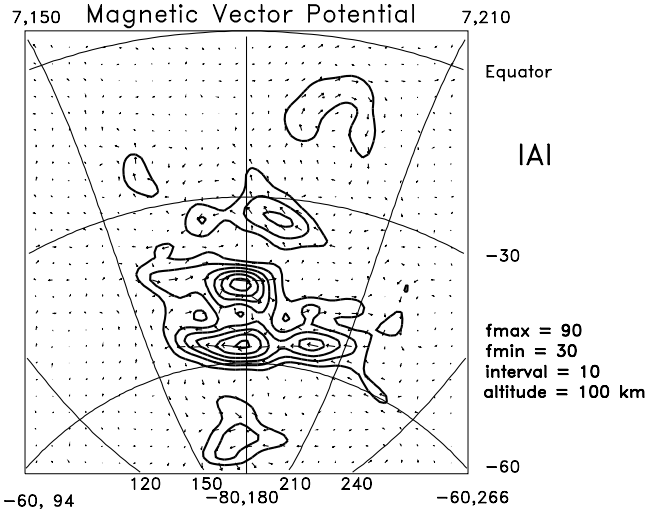

Figure 5. The magnetic vector potential plotted as a two-dimensional vector field with strongly positive magnitudes contoured. The field is extrapolated downward from 400 to 100 km. Map projection as in Figure 1.

We can choose the scalar field so that the vertical component of the vector potential is zero, then the vector potential is two-dimensional and can be plotted on a map. This representation suggests, because of sudden changes in direction, some sort of history. The vector potential extrapolated downward to 100 km (Figure 5) shows abrupt changes in direction which suggest different ages of magnetization or demagnetization for adjacent regions. The scalar potential does not hint at this.

[15] Finally, we argue that the vector potential, while more difficult to present, is more physically meaningful. The vector potential enters directly in Shroedinger's equation [*Baym*, 1969, pp. 74–79, 310–315] and would cause energy and angular momentum transitions and so magnetic realignments for capturing a thermal event. The scalar potential does not appear in this equation and so seems a just a convenient mathematical device: from a single scalar field the 3 components of the magnetic field are easily derived.

3. Summary

[16] We analyze Mars' crustal magnetic field in the heavily cratered southern highlands centered near latitude 40°S, longitude 180°W. We use ordinary two-dimensional Fourier analysis to vertically extrapolate from satellite mapping altitudes (400 km) to 100 km (aerobraking altitudes) or Mars' surface. The extrapolated field components are in excellent agreement with the aerobraking results [*Acuna et al.*, 1999] and provide a continuous representation of the field at that altitude, spanning the few aerobraking passes available in the region of interest. The field components can be used to construct magnetic scalar and vector potentials. These are smoother, in the sense that their derivatives generate the original field components, and these potentials are also simpler in the sense that fewer components are necessary to fully represent the magnetic field. Derived from the vertical

component of the magnetic field, the scalar potential is a scalar function whose gradient generates the two horizontal magnetic field components. We show that the agreement with the observed horizontal components is excellent. The scalar potential field at 400 km, satellite level, could be modeled using only 8 dipoles in the region analyzed; at 100 km, we show the fit for 14 dipoles (Figure 4b). More than 20 dipoles are required to model the surface field. The vector potential can be reduced to a two component horizontal field which can be plotted on a map as a set of arrows. This field shows abrupt lateral changes in direction and magnitude and suggests a history of magnetization which can be further analyzed.

[17] Major questions about the origin and nature of Mars' magnetism remain. Initially, the magnetization were interpreted as lineations with reversals [*Connerney et al.*, 1999] that could indicate a process like Earth's seafloor spreading on Mars. However, other interpretations have been made. *Cain et al.* [2003] constructed a 90 degree and order global spherical harmonic model of the scalar potential, and they note that choices for contouring and color strongly influence visual appearance and interpretation of magnetic patterns. They do not, however, specifically discuss this region in the southern hemisphere. In a planetary model fitted to aerobraking data (a 50 degree spherical harmonic analysis, downward continued to the surface), the strong magnetization in the southern hemisphere is interpreted in terms of equidimensional sources rather than lineations [*Arkani-Hamed*, 2001b]. Also, our models, Figures 4 and 5, depict small regions with intense magnetization. In an analysis of isolated magnetic regions for paleomagnetic pole determination, *Arkani-Hamed* [2001a] interprets adjacent regions with nearly 180° differences in magnetization directions as indicative of reversals of the field. The magnetic pattern we have analyzed in the southern hemisphere does not require reversed lineations, but does not exclude them either. Determination of past pole positions is beyond the scope of this paper.

[18] **Acknowledgments.** This project had its beginning with an exercise in *Claerbout*'s [1976] book on seismology in which the components of a two-dimensional (on a vertical plane) magnetic field along the upper boundary are obtained from the magnitude of the field using a Kolmogorov transform. Claerbout has disappeared, but the vector potential remains. The MGS mapping data set, binned by latitudes and longitudes, was the basis of our study; this was generously made available by J. Connerney and coauthors. We thank them for it. Also, we thank Michael D. Fuller and an anonymous reviewer, as well as Julianne Moses, for their careful reading of the submitted manuscript and their suggestions for improvements. We appreciate discussion with Peter Schultz and his continuing interest, and also the advice and assistance of Sarah Andre and Mark Robinson. We are grateful to NASA for funding from the Mars Data Analysis Program, grant NAG5-12157, that supported this research.

References

Acuna, M. H., et al. (1999), Global distribution of crustal magnetization discovered by the Mars Global Surveyor MAG/ER experiment, *Science*, *284*, 790–793.

Arkani-Hamed, J. (2001a), Paleomagnetic pole positions and pole reversals of Mars, *Geophys. Res. Lett.*, *17*, 3409–3412.

Arkani-Hamed, J. (2001b), A 50-degree spherical harmonic model of the magnetic field of Mars, *J. Geophys. Res.*, *106*, 23,197–23,208.

Baym, G. (1969), *Lectures on Quantum Mechanics*, 594 pp., W. A. Benjamin, White Plains, N. Y.

Blakely, R. J. (1996), *Potential Theory in Gravity and Magnetic Applications*, 441 pp., Cambridge Univ. Press, New York.

Cain, J. C., B. B. Ferguson, and D. Mozzoni (2003), An $n = 90$ internal potential function of the Martian crustal magnetic field, *J. Geophys. Res.*, *108*(E2), 5008, doi:10.1029/2000JE001487.

Claerbout, J. F. (1976), *Fundamentals of Geophysical Data Processing*, 274 pp., McGraw-Hill, New York.

Connerney, J. E. P., M. H. Acuna, P. J. Wasilewski, N. F. Ness, H. Rème, C. Mazelle, D. Vignes, R. P. Lin, D. L. Mitchell, and P. A. Cloutier (1999), Magnetic lineations in the ancient crust of Mars, *Science*, *284*, 794–798.

Connerney, J. E. P., M. H. Acuna, P. J. Wasilewski, G. Kletetschka, N. F. Ness, H. Reme, R. P. Lin, and D. L. Mitchell (2001), The global magnetic field of Mars and implications for crustal evolution, *Geophys. Res. Lett.*, *28*, 4015–4018.

Frey, H. V., J. H. Roark, K. M. Shockey, E. L. Frey, and S. E. H. Sakimoto (2002), Ancient lowlands on Mars, *Geophys. Res. Lett.*, *29*(10), 1384, doi:10.1029/2001GL013832.

Greeley, R., and J. E. Guest (1997), Geologic map of the eastern equatorial region of Mars, *U.S. Geol. Surv. Geol. Invest. Ser., Map I-1802-B*. (Reprinted in 1998.)

Kanasewich, E. R. (1975), *Time Series Analysis in Geophysics*, 364 pp., Univ. of Alberta Press, Alberta, Canada.

Langlais, B., M. E. Purucker, and M. Mandea (2004), Crustal magnetic field of Mars, *J. Geophys. Res.*, *109*, E02008, doi:10.1029/2003JE002048.

Mitchell, D. L., R. Lillis, P. Lin, J. Connerney, and M. Acuna (2003), Evidence for demagnetization of the Utopia impact basin on Mars, *Eos Trans. AGU*, *84*(46), Fall Meet. Suppl., Abstract GP22A-08.

Nimmo, F., and M. S. Gilmore (2001), Comments on the depth of magnetized crust on Mars from impact craters, *J. Geophys. Res.*, *106*, 11,315–11,323.

Parker, R. L. (2003), Ideal bodies for Mars magnetics, *J. Geophys. Res.*, *108*(E1), 5006, doi:10.1029/2001JE001760.

Rochette, P., L. Hood, G. Fillion, R. Ballou, and B. Ouladdiaf (2003), Impact demagnetization by phase transition on Mars, *Eos Trans. AGU*, *84*(50), 561.

Schultz, P. H., R. A. Schultz, and J. Rogers (1982), The structure and evolution of ancient impact craters on Mars, *J. Geophys. Res.*, *87*, 9803–9820.

Scott, D. H., and K. L. Tanaka (1997), Geologic map of the western equatorial region of Mars, *U.S. Geol. Surv. Geol. Invest. Ser., Map I-1802-A*. (Reprinted in 1998.)

Tanaka, K. L., and D. H. Scott (1997), Geologic map of the polar regions of Mars, *U.S. Geol. Surv. Geol. Invest. Ser., Map I-1802-C*. (Reprinted in 1998.)

D. M. Jurdy and M. Stefanick, Department of Geological Sciences, Northwestern University, 1850 Campus Drive, Evanston, IL 60208-2150, USA. (donna@earth.northwestern.edu)